THREE-DIMENSIONAL ANALYSIS OF LONGITUDINAL SPACE CHARGE MICROBUNCHING STARTING FROM SHOT NOISE*

D. Ratner, A. Chao, Z. Huang†

Stanford Linear Accelerator Center, Stanford, CA 94309, USA

Abstract

The commissioning of the Linac Coherent Light Source (LCLS) injector showed unexpected coherent optical transition radiation (COTR) for an uncompressed electron bunch downstream of a dog-leg transport line. In this paper, we develop a three-dimensional analysis of longitudinal space charge microbunching to explain the phenomenon. Our analysis takes into account the transverse correlation of the longitudinal space charge field due to shot-noise startup and finite observation angles of the radiation. We also apply this analysis to the LCLS COTR observations.

INTRODUCTION

In a linear accelerator for a high-gain free electron laser (FEL), a microbunching instability driven by various impedance effects can develop along the accelerator and may degrade the electron beam qualities that are critical for the FEL performance [1–8]. Longitudinal space charge (LSC) forces may dominate the instability gain for modulation wavelengths much shorter than the electron bunch length [5–8]. In the case of the high-brightness beam injector for the LCLS, COTR is detected from an uncompressed electron bunch downstream of a dog-leg transport line, indicating presence of microbunching at optical wavelengths [9].

At such short modulation wavelengths, electron shot noise is the most probable source of initial density fluctuations that could start the instability. Recently, Venturini noted [10] that the one-dimensional (1D) model of LSC impedance used in previous studies [5–8] may fail at very short wavelengths because the longitudinal modulations developed from shot noise may not be uniform in transverse directions. In this paper, we present a three-dimensional (3D) analysis of LSC microbunching starting from shot noise. Using a simplified machine model motivated by the LCLS setup, we calculate the microbunching gain factor for short modulation wavelengths observed at small angles relative to the longitudinal direction. We also compare these results with the LCLS COTR observations [11].

3D ANALYSIS

We consider an electron bunch that is very long compared to the modulation wavelengths under study. At a relativistic energy, we ignore the transverse space charge

force (because of the cancelation between the electric and magnetic self-fields) and assume that the electrons' relative longitudinal positions are frozen until reaching a dispersive beamline element. The random distribution of electrons in the bunch produces LSC fields, which in turn cause energy modulations to accumulate along the accelerator. A dispersive element with nonzero momentum compaction can then convert the energy modulation to longitudinal position changes. As a result, the longitudinal density distribution is modified from the initial random distribution and may show enhancement at some frequency range, i.e., the beam is microbunched at these frequencies.

Longitudinal Space Charge Field

We calculate the longitudinal space charge field by summing over contributions from N point charges at (x_j, y_j, z_j) $(j = 1, 2, ..., N)$:

$$E_z(\boldsymbol{x}) = \frac{e}{4\pi\epsilon_0} \sum_j^N \frac{\gamma_0(z-z_j)}{[(x-x_j)^2 + (y-y_j)^2 + \gamma_0^2(z-z_j)^2]^{3/2}},$$

(1)

where $\boldsymbol{x} = (x, y, z)$, and $\gamma_0 mc^2$ is the average electron energy as the beam energy spread is assumed to be small. The longitudinal Fourier transform of E_z is

$$\tilde{E}_k(\boldsymbol{r}) = \int_{-\infty}^{\infty} dz E_z(x, y, z) e^{-ikz}$$

$$= \frac{-eik}{2\pi\gamma_0^2\epsilon_0} \sum_j^N e^{-ikz_j} K_0\left(\frac{k|\boldsymbol{r} - \boldsymbol{r}_j|}{\gamma_0}\right),$$

(2)

where $\boldsymbol{r} = (x, y)$ represents the transverse coordinates, $k = 2\pi/\lambda$ is the modulation wavenumber, and K_0 is the modified Bessel function.

$\tilde{E}_k$ is a fluctuating quantity derived from shot noise of the beam. As we will see in the following sections, the microbunching gain and COTR intensity are related to the ensemble average

$$\left\langle \tilde{E}_k(\boldsymbol{r}_1)\tilde{E}_k^*(\boldsymbol{r}_2) \right\rangle = \left(\frac{ek}{2\pi\epsilon_0\gamma_0^2}\right)^2$$

$$\times \left\langle \sum_{j=1}^N K_0\left(\frac{k|\boldsymbol{r}_1 - \boldsymbol{r}_j|}{\gamma_0}\right) K_0\left(\frac{k|\boldsymbol{r}_2 - \boldsymbol{r}_j|}{\gamma_0}\right) \right\rangle.$$

(3)

Here we have assumed that the beam is initially uncorrelated at the modulation wavelength λ. For a given trans-
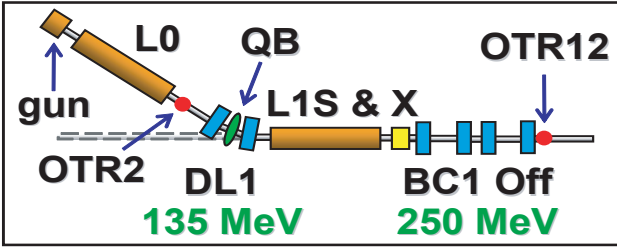
Figure 1: LCLS injector layout showing OTR2, DL1 and OTR12 for the COTR experiment when BC1 is off.

verse distribution, $\rho(\boldsymbol{r})$, Eq. (3) becomes

$$
\begin{aligned}
\left\langle \tilde{E}_k(\boldsymbol{r}_1)\tilde{E}_k^*(\boldsymbol{r}_2) \right\rangle &= N \left(\frac{ek}{2\pi\epsilon_0\gamma_0^2} \right)^2 \\
&\times \int d\boldsymbol{r}\,\rho(\boldsymbol{r}) K_0\left(\frac{k|\boldsymbol{r}_1 - \boldsymbol{r}|}{\gamma_0} \right) K_0\left(\frac{k|\boldsymbol{r}_2 - \boldsymbol{r}|}{\gamma_0} \right).
\end{aligned} \quad (4)
$$

In the following analysis, we take a round Gaussian beam for the normalized transverse distribution:

$$
\rho(\boldsymbol{r}) = \frac{1}{2\pi\sigma_x^2} \exp\left(-\frac{x^2 + y^2}{2\sigma_x^2} \right), \quad (5)
$$

where $\sigma_x(=\sigma_y)$ is the rms transverse beam size.

Microbunching Gain when $k\sigma_x/\gamma_0 \gg 1$

In this section, we will focus on the analysis of the microbunching gain in the high-frequency limit when $k\sigma_x/\gamma_0 \gg 1$. This condition is approximately satisfied by the LCLS injector when the modulation wavelength is in the optical regime and γ_0 is not too large. In this limit, the average LSC field scales inversely with transverse beam size because

$$
\int d\boldsymbol{r}_1\rho(\boldsymbol{r}_1) \int d\boldsymbol{r}_2\rho(\boldsymbol{r}_2) \left\langle \tilde{E}_k(\boldsymbol{r}_1)\tilde{E}_k^*(\boldsymbol{r}_2) \right\rangle \propto \frac{1}{k^2\sigma_x^4}
$$

and does not depend on γ_0. Thus, LSC dominates in the beamline section where the transverse beam size is smallest. In the LCLS injector, the electron beam forms a narrow waist at OTR2. For a simplified treatment, we consider the LSC contribution to be localized at this waist and calculate the bunching factor at the observation point (OTR12) after a dog-leg transport line (DL1, see Fig. 1). A more general study that integrates the LSC contribution along the electron trajectory will be discussed elsewhere [12].

We use $\delta_0 = (\gamma - \gamma_0)/\gamma_0$ to denote an electron's initial energy deviation. After the LSC interaction at the waist region, the energy becomes $\delta = \delta_0 + \delta_m$, where δ_m is the relative energy modulation due to LSC,

$$
\delta_m(\boldsymbol{x}_0) = \frac{eE_z(\boldsymbol{x}_0)L_d}{\gamma_0 mc^2}, \quad (6)
$$

and L_d is the effective interaction length at the waist.

After this short LSC interaction section, the subsequent electron motion is determined by the linear transfer matrix

FEL Technology

that includes the dispersive element (DL1 in the LCLS case). Thus, the electron coordinates at the observation point (OTR12) are given by

$$
\begin{aligned}
x &= R_{11}x_0 + R_{12}x_0' + R_{16}\delta, \\
y &= R_{33}y_0 + R_{34}y_0', \\
z &= z_0 + R_{51}x_0 + R_{52}x_0' + R_{56}\delta,
\end{aligned} \quad (7)
$$

where the index 0 refers to the LSC section, and x' and y' refer to transverse angles of the electron. R_{51} and R_{52} are zero for a linearly achromatic transfer line, but they can be nonzero when the quadrupole inside DL1 (QB) is purposely mistuned to suppress microbunching, as performed in the LCLS experiments [9, 11]. Because R_{16} is small when DL1 is close to the achromatic condition and the initial energy spread is also small, we drop $R_{16}\delta$ in comparison with other two beam size terms in the first line of Eq. (7). Higher-order transport effects are neglected here and will be discussed in the final section.

In a typical OTR setup, a camera collects the OTR signal over a finite angle relative to the forward direction of the radiation. We calculate the bunching factor for a modulation wavenumber k observed at small angles (θ_x, θ_y) relative to the longitudinal direction:

$$
b(\boldsymbol{k}) = \frac{1}{N} \sum_{j=1}^{N} e^{-i\boldsymbol{k}\cdot\boldsymbol{x}(\boldsymbol{X}_{0j})}, \quad (8)
$$

where $\boldsymbol{k} \approx (k\theta_x, k\theta_y, k)$, and

$$
\boldsymbol{X}_{0j} = (x_{0j}, x_{0j}', y_{0j}, y_{0j}', z_{0j}, \delta_{0j}) \quad (9)
$$

is the 6D phase space position of the jth electron just before the LSC interaction. The OTR intensity is related to the ensemble average of the bunching factor given by

$$
\langle |b(\boldsymbol{k})|^2 \rangle = \frac{1}{N} + \frac{1}{N^2} \sum_{j=1}^{N}\sum_{l\neq j}^{N} e^{i\boldsymbol{k}\cdot[\boldsymbol{x}(\boldsymbol{X}_{0l}) - \boldsymbol{x}(\boldsymbol{X}_{0j})]}. \quad (10)
$$

The first term gives the incoherent bunching, while the second term gives the coherent bunching. Focusing on the coherent bunching contribution, we can turn the sum of Eq. (8) into an integration over the smoothed electron distribution function $f_0(\boldsymbol{X}_0)$,

$$
b_c(\boldsymbol{k}) = \frac{1}{N} \int d^6\boldsymbol{X}_0 f_0(\boldsymbol{X}_0) e^{-i\boldsymbol{k}\cdot\boldsymbol{x}(\boldsymbol{X}_0)}. \quad (11)
$$

In view of Eq. (7), the exponent of Eq. (11) is

$$
\begin{aligned}
\boldsymbol{k}\cdot\boldsymbol{x} &= kz + k\theta_x x + k\theta_y y = k\Big[z_0 + R_{56}(\delta_0 + \delta_m) \\
&\quad + R_1 x_0 + R_2 x_0' + \theta_y R_{33} y_0 + \theta_y R_{34} y_0' \Big],
\end{aligned} \quad (12)
$$

where we have defined

$$
\begin{aligned}
R_1 &\equiv R_{51} + \theta_x R_{11}, \\
R_2 &\equiv R_{52} + \theta_x R_{12}.
\end{aligned} \quad (13)
$$

Treating the LSC-induced energy modulation as a small perturbation and expanding Eq. (11) to first-order in δ_m, we have

$$b_c(\boldsymbol{k}) \approx \frac{1}{N} \int d^6 X_0 f_0(\boldsymbol{X}_0) \left[1 - ikR_{56}\delta_m(\boldsymbol{x}_0)\right] e^{-ikz_0}$$
$$\times e^{-ik\left[R_{56}\delta_0 + R_1 x_0 + R_2 x_0' + \theta_y(R_{33}y_0 + R_{34}y_0')\right]}. \quad (14)$$

Note that $\delta_m(\boldsymbol{x}_0)$ contains the fast z_0 oscillation (high-frequency LSC modulation) but also depends on the transverse coordinates x_0 and y_0 from Eq. (6). The initial average beam distribution is assumed to be Gaussian in transverse and energy variables, and uniform longitudinally with a line density n_0:

$$f_0(\boldsymbol{X}_0) = \frac{n_0}{(2\pi\sigma_{x0}\sigma_{x0'})^2 \sqrt{2\pi}\sigma_{\delta 0}}$$
$$\times \exp\left[-\frac{(\delta_0 - \delta_{0c}(z_0))^2}{2\sigma_{\delta 0}^2} - \frac{x_0^2 + y_0^2}{2\sigma_{x0}^2} - \frac{x_0'^2 + y_0'^2}{2\sigma_{x0'}^2}\right], \quad (15)$$

where $\sigma_{\delta 0}$ is the rms slice energy spread, δ_{0c} is the initial energy-z correlation, and $\sigma_{x0'}$ is the rms angular divergence. The transverse emittances at the waist are $\epsilon_y = \epsilon_x = \sigma_{x0}\sigma_{x0'}$.

Inserting Eq. (15) to Eq. (14) and defining a new energy variable

$$\delta_{0u} = \delta_0 - \delta_{0c}(z_0), \quad (16)$$

Eq. (14) becomes

$$b_c(\boldsymbol{k}) = \frac{1}{N} \int dx_0 dx_0' dy_0 dy_0' dz_0 d\delta_{0u} f_0(\boldsymbol{X}_0)$$
$$\times \left[-ikR_{56}\delta_m(x_0, y_0, z_0)\right] e^{-ik[z_0 + R_{56}\delta_{0c}(z_0)]}$$
$$\times e^{-ik[R_{56}\delta_{0u} + R_1 x_0 + R_2 x_0' + \theta_y(R_{33}y_0 + R_{34}y_0')]}. \quad (17)$$

For simplicity, we assume the correlated energy spread δ_{0c} is small and take $z_0 + R_{56}\delta_{0c}(z_0) \approx z_0$. (A linear chirp $\delta_{0c} = hz_0$ will compress the modulation wavelength, as in Refs. [3, 4].) Inserting Eq. (6) to (17), we use the z_0 integration to switch E_z to $\tilde{E}_k$. After carrying out δ_{0u}, x_0', and y_0' integrations, we obtain

$$b_c(\boldsymbol{k}) = \frac{n_0}{N}\left(\frac{-iekR_{56}L_d}{\gamma_0 mc^2}\right)$$
$$\times \exp\left[-\frac{k^2 R_{56}^2 \sigma_{\delta 0}^2}{2} - \frac{k^2(R_2^2 + \theta_y^2 R_{34}^2)\sigma_{x0'}^2}{2}\right]$$
$$\times \int d\boldsymbol{r}_0 \tilde{E}_k(\boldsymbol{r}_0) e^{-ik(R_1 x_0 + \theta_y R_{33}y_0)}\rho(\boldsymbol{r}_0). \quad (18)$$

Using Eqs. (4) and (5) and taking the high-frequency limit $k\sigma_{x0}/\gamma_0 \gg 1$, we can show [12]

$$\int d\boldsymbol{r}_1 \rho(\boldsymbol{r}_1) \int d\boldsymbol{r}_2 \rho(\boldsymbol{r}_2)$$
$$\times \langle E_k(\boldsymbol{r}_1)E_k^*(\boldsymbol{r}_2)\rangle e^{-ik[R_1(x_1-x_2) + \theta_y R_{33}(y_1-y_2)]}$$
$$\approx \left(\frac{e}{2\pi\epsilon_0}\right)^2 \frac{N}{3k^2\sigma_{x0}^4} \frac{1}{\left[1 + \gamma_0^2(R_1^2 + \theta_y^2 R_{33}^2)\right]^2}. \quad (19)$$

Thus, the ensemble average of the coherent bunching is

$$\langle|b_c(\boldsymbol{k})|^2\rangle \approx \frac{4}{3N}\left[\frac{I_0(z_0)}{\gamma_0 I_A}\frac{R_{56}L_d}{\sigma_{x0}^2}\right]^2$$
$$\times \frac{\exp\left[-k^2 R_{56}^2 \sigma_{\delta 0}^2 - k^2(R_2^2 + \theta_y^2 R_{34}^2)\sigma_{x0'}^2\right]}{\left[1 + \gamma_0^2(R_1^2 + \theta_y^2 R_{33}^2)\right]^2}, \quad (20)$$

where $I_0 = ecn_0$ is the electron bunch current, and $I_A = ec/r_e \approx 17$ kA is the Alfven current. Equation (20) determines the microbunching gain in presence of chromatic effects and finite observation angles for a localized LSC interaction in the high-frequency limit. The LSC field starting from shot noise is transversely correlated only within $\gamma_0\lambda/(2\pi)$ instead of the full transverse beam size σ_{x0} [10], hence the gain suppression due to nonzero R_{51} and/or observation angles does not involve the transverse beam size.

OTR Intensity

The OTR intensity can be shown to have spectral and angular dependence

$$\frac{d^2W}{d\omega d\Omega} = \left(\frac{d^2W}{d\omega d\Omega}\right)_1 \left[N + N^2|b_c(\boldsymbol{k})|^2\right]. \quad (21)$$

Here the single-electron transition-radiation angular distribution is

$$\left(\frac{d^2W}{d\omega d\Omega}\right)_1 \propto \frac{\gamma_f^4(\theta_x^2 + \theta_y^2)}{\left[1 + \gamma_f^2(\theta_x^2 + \theta_y^2)\right]^2}, \quad (22)$$

where $\gamma_f mc^2$ is the electron energy at the OTR screen, and the observation angles $\theta_{x,y} \ll 1$. From Eq. (21), the OTR intensity can be calculated by integrating over the camera collection angle θ_m as

$$\frac{dW}{d\omega} = \int_{-\theta_m/2}^{\theta_m/2} d\theta_x \int_{-\theta_m/2}^{\theta_m/2} d\theta_y$$
$$\times \left(\frac{d^2W}{d\omega d\Omega}\right)_1 \left[N + N^2|b_c(\boldsymbol{k})|^2\right]. \quad (23)$$

The first term in the square bracket is the incoherent OTR, while the second term is the coherent OTR due to microbunching. The OTR spectral gain is the ratio of the angle-integrated second term to the angle-integrated first term.

COMPARISON WITH THE LCLS OBSERVATIONS

The LCLS COTR observations in the absence of compression was initially described in Ref. [9] (see Fig. 44 and the paragraph above it). After these initial observations, a transmission grating spectrometer was installed in OTR12 to study COTR spectral content, and more data were collected in 2008 at 250 pC bunch charge [11]. One such result is shown in Fig. 2. The integrated OTR signal maximizes
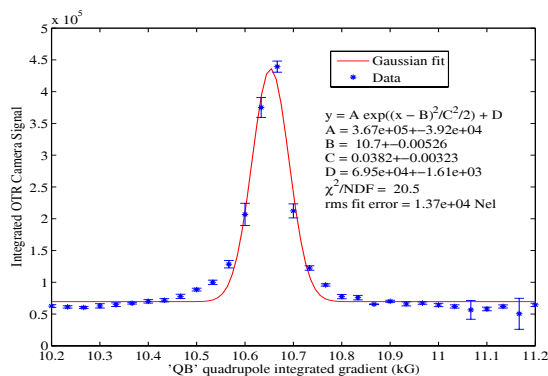
Figure 2: The integrated OTR signal as a function of the QB quadrupole strength at 250 pC bunch charge (courtesy D. Dowell *et al.*).

Figure 3: Measured and calculated OTR intensity gain for 250 pC charge at OTR12 as a function of the optical wavelength.

at the QB quadrupole setting that makes the DL1 bend system a perfect linear achromat (see Fig. 1). When QB is set off peak, the microbunching is washed out by nonzero R_{51} and R_{52} of the nonachromatic bend system.

During this study, single-shot spectral data were also collected at QB = 10.67 kG (peak COTR intensity) and at QB = 11 kG (baseline incoherent level). Analyzing the spectral data and taking the ratio of the two spectra, we obtain the OTR intensity gain as a function of the optical wavelength, shown in Fig. 3. We then use the experimental beam parameters to determine the theoretical gain curve. We take $\gamma_0 mc^2 = 135$ MeV, $\gamma_0 \epsilon_{x,y} = 1$ μm, $\beta_0 = 1.2$ m, and the effective interaction length $L_d \approx 2.5$ m for the beam waist extending ± 2 m from the waist at OTR2. The momentum compaction of DL1 is $R_{56} = 6.3$ mm when it is set to be achromatic. The electron bunch peak current is $I_0 \approx 40$ A for a 250 pC charge with an rms bunch length of 750 μm, the electron energy at OTR12 is $\gamma_f mc^2 = 250$ MeV, and the maximum OTR collection angle is $\theta_m = 75$ mrad. Using these parameters, $k\sigma_{x_0}/\gamma_0 \geq 2$ for $\lambda \leq 1$ μm, and hence the high-frequency approximation is reasonable. We calculate the spectral gain using Eqs. (20) and (23) by setting $R_{51} = R_{52} = 0$ and using R_{11}, R_{12}, R_{33}, R_{34} from the LCLS design lattice. Because the gain depends sensitively on the slice energy spread $\sigma_{\delta 0}$ (undetermined from the experiment), we compute three theoretical gain curves using a slice rms energy spread of 2, 3, and 4 keV, respectively. As shown in Fig. 3, the theoretical gain curve for a slice rms energy spread of 3 keV fits well with the experimental result. The 3 keV value is consistent with the typical slice energy spread expected from the LCLS photocathode rf gun and the measured level from the TESLA Test Facility photocathode gun [13].

We also use Eqs. (20) and (23) at different QB settings to calculate the width of the QB curve at $\lambda = 1$ μm, the dominant COTR wavelength within the OTR camera's bandwidth. The absence of the transverse beam size (σ_{x0}) in the second line of Eq. (20) reduces QB sensitivity, but we still predict a width about a factor of 2 narrower than in the measured QB curve (Fig. 2). We suspect the larger experi-

mental QB width may be related to the non-smooth transverse electron distribution generated by laser and/or cathode nonuniformity.
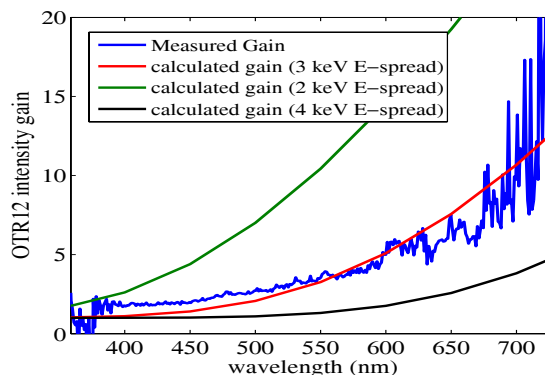
DISCUSSIONS

In this paper, we show that longitudinal space charge microbunching starting from shot noise can explain the LCLS COTR observations in the absence of compression. Our analysis takes into account the limited transverse correlation of the longitudinal space charge field due to shot noise startup and finite observation angles of the radiation. Subsequent experiments at the LCLS indicate that such short wavelength microbunching may also be sensitive to nonlinear transport effects when beam energy spread and/or angular spread are relatively large, and further studies continue.

We thank the LCLS commissioning team for sharing the COTR experimental results and stimulating discussions.

REFERENCE

[1] M. Borland et al., Nucl. Instrum. Meth. A **483**, 268 (2002).

[2] E. Saldin, E. Schneidmiller, M. Yurkov, Nucl. Instrum. Meth. A **490**, 1 (2002).

[3] S. Heifets, G. Stupakov, S. Krinsky, Phys. Rev. ST-AB **5**, 064401 (2002).

[4] Z. Huang, K.-J. Kim, Phys. Rev. ST-AB **5**, 074401 (2002).

[5] E. Saldin, E. Schneidmiller, M. Yurkov, Nucl. Instrum. Meth. A **528**, 355 (2004).

[6] Z. Huang *et. al.*, Phys. Rev. ST-AB **7**, 074401 (2004).

[7] T. Shaftan, Z. Huang, Phys. Rev. ST-AB 7, 080702 (2004).

[8] M. Venturini, Phys. Rev. ST-AB **10**, 104401 (2007).

[9] R. Akre *et. al.*, Phys. Rev. ST-AB **11**, 030703 (2008).

[10] M. Venturini, Phys. Rev. ST-AB **11**, 030703 (2007).

[11] H. Loos *et. al.*, these FEL2008 Proceedings.

[12] D. Ratner *et. al.*, to be published.

[13] M. Hüning and H. Schlarb, PAC2003 Proceedings, 2074 (2003).

FEL Technology